Cellular Microbiology (2015) **17**(11), 1583–1593
doi:10.1111/cmi.12457
First published online 28 May 2015

Two polar residues within C-terminal domain of M1 are critical for the formation of influenza A Virions

Ke Zhang,[1†] Zhao Wang,[2,3†] Gui-Zhen Fan,[2] Juan Wang,[4] Shengyan Gao,[1] Yun Li,[1] Lei Sun,[1] Chang-Cheng Yin,[2*] Wen-Jun Liu[1,5]**

[1]*Center for Molecular Virology, CAS Key Laboratory of Pathogenic Microbiology and Immunology, Institute of Microbiology, Chinese Academy of Sciences, Beijing 100101, China.*

[2]*Department of Biophysics, Health Science Center, Peking University, Beijing 100191, China.*

[3]*National Center for Macromolecular Imaging, Verna and Marrs McLean Department of Biochemistry and Molecular Biology, Baylor College of Medicine, Houston, TX 77030, USA.*

[4]*Department of Molecular Biology, University of Texas Southwestern Medical Center, Dallas, TX 75390, USA.*

[5]*Center for Influenza Research and Early-warning, Chinese Academy of Sciences, Beijing 100101, China.*

Summary

The matrix protein 1 (M1) is the most abundant structural protein in influenza A virus particles. It oligomerizes to form the matrix layer under the lipid membrane, sustaining stabilization of the morphology of the virion. The present study indicates that M1 forms oligomers based on a fourfold symmetrical oligomerization pattern. Further analysis revealed that the oligomerization pattern of M1 was controlled by a highly conserved region within the C-terminal domain. Two polar residues of this region, serine-183 (S183) and threonine-185 (T185), were identified to be critical for the oligomerization pattern of M1. M1 point mutants suggest that single S183A or T185A substitution could result in the production of morphologically filamentous particles, while double substitutions, M1-S183A/T185A, totally disrupted the fourfold symmetry and resulted in the failure of virus production. These data indicate that the polar groups in these residues are essential to control the oligomerization pattern of M1. Thus, the present study will aid in determining the mechanisms of influenza A virus matrix layer formation during virus morphogenesis.

Received 25 August, 2014; revised 24 April, 2015; accepted 28 April, 2015. For correspondence. *E-mail: ccyin@hsc.pku.edu.cn; Tel. (+86) 10 6275 8127; Fax (+86) 10 6275 3790; **E-mail: liuwj@im.ac.cn; Tel. (+86) 10 6480 7497; Fax (+86) 10 6480 7503.
[†]These authors contributed equally to this work.

Introduction

Influenza viruses are enveloped viruses that belong to the family Orthomyxoviridae (Heggeness *et al.*, 1982; Lamb and Choppin, 1983; Enami *et al.*, 1985). The genome of influenza A virus contains eight negative-sense RNA segments that code for at least 11 proteins.

The M1, encoded by the M segment, is comprised of 252 amino acids (Shaw *et al.*, 2008). M1 is an α-helical protein and consists of two domains. The three-dimensional structure of the N-terminal (1–164 aa) domain has been obtained by X-ray diffraction at pH 4.0 and 7.0 (Sha and Luo, 1997a,b; Arzt *et al.*, 2001; Harris *et al.*, 2001). The C-terminal domain (165–252 aa) contains an appreciably unstructured region, so the atomic structure of the M1 C-terminal domain has not been determined (Shishkov *et al.*, 1999; 2009; 2011; Arzt *et al.*, 2001; Ksenofontov *et al.*, 2011).

The M1 is a multifunctional protein that plays an important role in the virus life cycle. Previous investigations demonstrated that M1 has a strong tendency to oligomerize (Bui *et al.*, 2000) and this oligomerization is essential for the formation of matrix layer during virus assembly and budding processes (Avalos *et al.*, 1997; Ali *et al.*, 2000; Gomez-Puertas *et al.*, 2000; Barman *et al.*, 2001; Latham and Galarza, 2001; Wang *et al.*, 2010). The matrix layer, which exists in many enveloped viruses, links the viral envelope and the virus core. The structure of the matrix layer and the arrangement of matrix proteins in the matrix layer have been studied in several viruses. The M protein forms a helical structure of matrix layer in vesicular stomatitis virus; the M helix forms a triangularly packed lattice of M subunits (Ge *et al.*, 2010). The matrix layer in Newcastle disease virus (NDV) forms a grid-like array generated by repeating matrix subunits whose appearance is nearly square-shaped (Battisti *et al.*, 2012). The M protein of measles virus forms a left-handed helix with a pitch of 7.2 nm (Liljeroos *et al.*, 2011). The formation of matrix layer is a critical step for the budding process and generation of mature viral particles of influenza A virus (Nayak *et al.*, 2009). The oligomerization of M1 under the

lipid membrane causes asymmetry in the lipid bilayer, thereby facilitating membrane bending required for budding initiation. In addition, M1 oligomerization appears to be a critical component in the final step of budding closure, causing virion release (Ruigrok *et al*., 2000; Nayak *et al*., 2004; 2009; Rossman *et al*., 2010). A previous study showed that the N-terminus mediates the oligomerization of M1 and the oligomerization of M1 at the budding site controls the morphology of the viral particles (Sha and Luo, 1997a,b; Harris *et al*., 2001; Noton *et al*., 2007). Some key residues of M1 that important to the morphology of the virions were identified in both N-terminal and C-terminal domains by previously studies (Elleman *et al*., 2004; Burleigh *et al*., 2005; Bialas *et al*., 2012). Nevertheless, no three-dimensional structure of M1 oligomer has previously been obtained. Therefore, the molecular mechanism of M1 oligomerization is not well understood.

To resolve these aforementioned issues, in the present study, a 580 kDa M1 oligomer was collected and the molecular mechanism of M1 oligomerization was determined. The results showed that the M1 oligomer displays fourfold symmetry. The oligomerization pattern of M1 was controlled by a highly conserved region within the C-terminal domain. Two polar residues, serine-183 (S183) and threonine-185 (T185), were identified as the key residues. Alanine substitution mutation of either of the two residues could affect the morphology of the virion particles.

Results

M1 oligomers display fourfold symmetry

Previous studies demonstrated that recombinant M1 protein, which was expressed and purified from *Escherichia coli*, can oligomerize at neutral pH *in vitro*. After nickel affinity chromatography and gel filtration, the protein was concentrated to 0.5 mg ml^{-1} and was reloaded on the gel filtration column. Four fractions (15.8, 13.5, 11.2 and 10.1 ml), whose molecular masses were determined to be 55, 155, 460 and 580 kDa, appeared on the column at neutral pH (Zhang *et al*., 2012). To gain a better understanding of the molecular mechanism of M1 oligomerization, higher order multimers were the focus of this study. The M1 oligomers collected from the 10.1 ml fraction were visualized by negative staining electron microscopy. A total of 200 images for individual M1 particles were obtained, boxed out and classified using EMAN 1.8 (Fig. 1A) and the symmetry of the particles was determined by reference free two-dimensional classification analysis. After single particle analysis processing, the selected class average revealed that M1 particles form a tetrameric ring conformation displaying fourfold symmetry (Fig. 1B).

Previously studies also showed that the N-terminal domain of M1 (M1N) could oligomerizes at pH 7.4 (Harris *et al*., 2001; Zhang *et al*., 2012). Recombinant N-terminal of M1 protein, which was expressed and purified from *E. coli*, was purified by nickel affinity chromatography and gel filtration. The purified protein was concentrated to 0.5 mg ml^{-1} and was reloaded on the gel filtration column. The elution volumes of the fractions were 9.8, 11.3, 13.5, 16.0 and 17.6 ml, corresponding to the molecular masses of 654, 436, 169, 51 and 19 kDa respectively (Zhang *et al*., 2012). Then the oligomerization pattern of N-terminal domain was analysed by negative staining electron microscopy. The electron microscopy data of M1N oligomers were collected following the same procedure used for the full-length protein. In total,

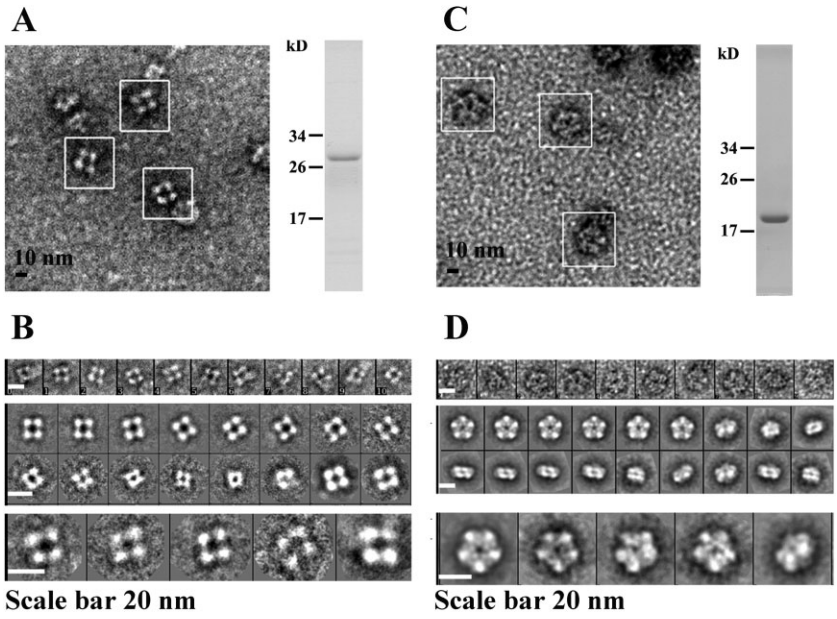

Fig. 1. The oligomerization pattern of M1 and its N-terminal domain. The 10.1 ml fraction of M1 and 9.8 ml fraction of M1N obtained from gel filtration (pH 7.4) were analysed by negative staining electron microscopy. Representative micrograph of protein particles (indicated by the white box): M1 (A), M1N (C). The purified proteins were analysed by SDS-PAGE. Selected particles of M1 (B) and M1N (D) were followed by initial processing with EMAN1.8. A range of two-dimensional class averages (50 particles per class) and eigenimages reveal the fourfold symmetry of M1 and fivefold symmetry of M1N in the entire data set.

150 images of the 9.8 ml M1N fraction were collected and were processed using EMAN 1.8 (Fig. 1C). Intriguingly, M1N particles appeared as pentameric rings displaying fivefold symmetry (Fig. 1D).

A recent study showed that the C-terminal domain of M1 plays a key role in the formation of M1 supramolecular structure (Shtykova *et al.*, 2013). In the present study, the results demonstrate that M1 forms fourfold symmetrical oligomers and that M1N forms oligomers with fivefold symmetry. Thus, we infer that the C-terminal domain of M1 is critical to control the self-oligomerization pattern of the full-length protein.

S183 and T185 are key residues for the oligomerization pattern of M1

To identify the region in the C-terminal domain that is important to the oligomerization pattern of intact M1, several truncations of the C-terminal domain were constructed. The largest elution volumes of M1(1–244 aa), M1(1–232 aa), M1(1–224 aa), M1(1–212 aa), M1(1–193 aa) and M1(1–180 aa) on the gel filtration column at pH 7.4 were 15.6, 15.7, 15.8, 16.0, 16.5 and 17.3 ml, corresponding to apparent molecular masses of 56.2, 53.7, 51.3, 46.8, 39.2 and 26.9 kDa respectively (Fig. 2A). With the exception of M1 (1–180 aa), which appeared to be a monomer, the calculated molecular masses of all of the other truncations were double their theoretical value, indicating that residues 180–193 were important to the dimerization of the intact protein (Fig. 2A). The sequences alignment showed that this region is highly conserved in all of the sequences investigated (Fig. 2B). To determine the key residue(s) for the dimerization of M1, point mutation experiments were performed. Each residue in the dimerization region (181–193 aa, except alanine) was individually substituted with alanine. The oligomerization states of the purified, mutated M1 proteins were also analysed by gel filtration at pH 7.4. The result showed that the largest elution volume of wild-type M1 protein was 15.8 ml, whose molecular mass was 52 kDa, indicating that the smallest oligomerization unit of wild-type M1 was dimer. The smallest oligomerization units of M1-L181A, M1-T184A, M1-K187A, M1-189A, M1-E190A, M1-Q191A, M1-M192A were also eluted at 15.8 ml, remaining the same as wild-type M1 proteins. But the largest elution volumes of mutant proteins, which lack residues with hydroxyl side chains: M1-S183A and M1-T185A, were shifted to 17.2 ml. The molecular mass of this fraction was calculated to be 29 kDa, nearly identical to monomeric M1. The smallest oligomerization unit of the double-point mutant M1-S183A/T185A was also eluted at 17.2 ml. (Fig. 2C). These results demonstrated that the S183A and T185A mutations altered the smallest oligomerization state of M1, resulting in elution volume shift in gel filtration column and production of monomeric proteins.

We next analysed if the point mutations could disrupt the self-oligomerization pattern of M1. The 9.8 ml gel filtration column fraction (pH 7.4) of each mutated M1 was collected and analysed by negative staining electron microscopy. Two hundred oligomeric particles from M1-S183A, or M1-T185A or M1-S183A/T185A were obtained, boxed out and processed by following the same procedure as the full-length protein. Representative particles and the ratio of different symmetric particles were exhibited. Because both M1-S183A and M1-T185A mutants could form 15.8 and 17.2 ml fractions (Fig. 2C), the results showed that there were two types of oligomerization pattern found in M1-S183A and M1-T185A oligomers. A total of 50% of the M1-S183A particles displayed fourfold symmetry, the other half displayed fivefold symmetry (Fig. 2D). A total of 67% of the M1-T185A particles displayed fourfold symmetry, while 33% of other particles (Fig. 2E) were in fivefold symmetry. In contrast, 100% of the M1-S183A/T185A particles displayed fivefold symmetry (Fig. 2F). Oligomers of other mutants all exhibited fourfold symmetry (data not shown). These results confirmed that dimerization of M1 is directly related to its oligomerization pattern and that the proper oligomerization of M1 is based on its ability to dimerize.

S183 and T185 are important for the morphology of virions

To examine if the S183 and T185 residues are critical for virus viability, we generated viruses possessing mutant M1 using plasmid-based reverse genetic system for A/WSN/1933 (WSN). The single alanine substitution mutation of either of these positions (WSN-M1-S183A and WSN-M1-T185A) did not affect virus generation. However, the double-point mutations at S183 and T185 with alanine did not support virus generation. To further characterize the single-point M1 mutants, the growth kinetics of these viruses were determined using Darby Canine Kidney Epithelial Cells (MDCK) cells. There was no obvious difference between wild-type virus and WSN-M1-S183A or WSN-M1-T185A mutant virus in the growth curves (Fig. 3A). Furthermore, the expression levels of M1 and nucleoprotein (NP) were not significantly affected (Fig. 3B). These data confirmed that the single-point mutations of S183 and T185 did not remarkably affect the virus replication process.

To further examine the architecture of the patches at the cell periphery, virus-infected cells were analysed using transmission electron microscopy at 16 h post-infection. Uninfected cells were used as control (Fig. 4A). In cells

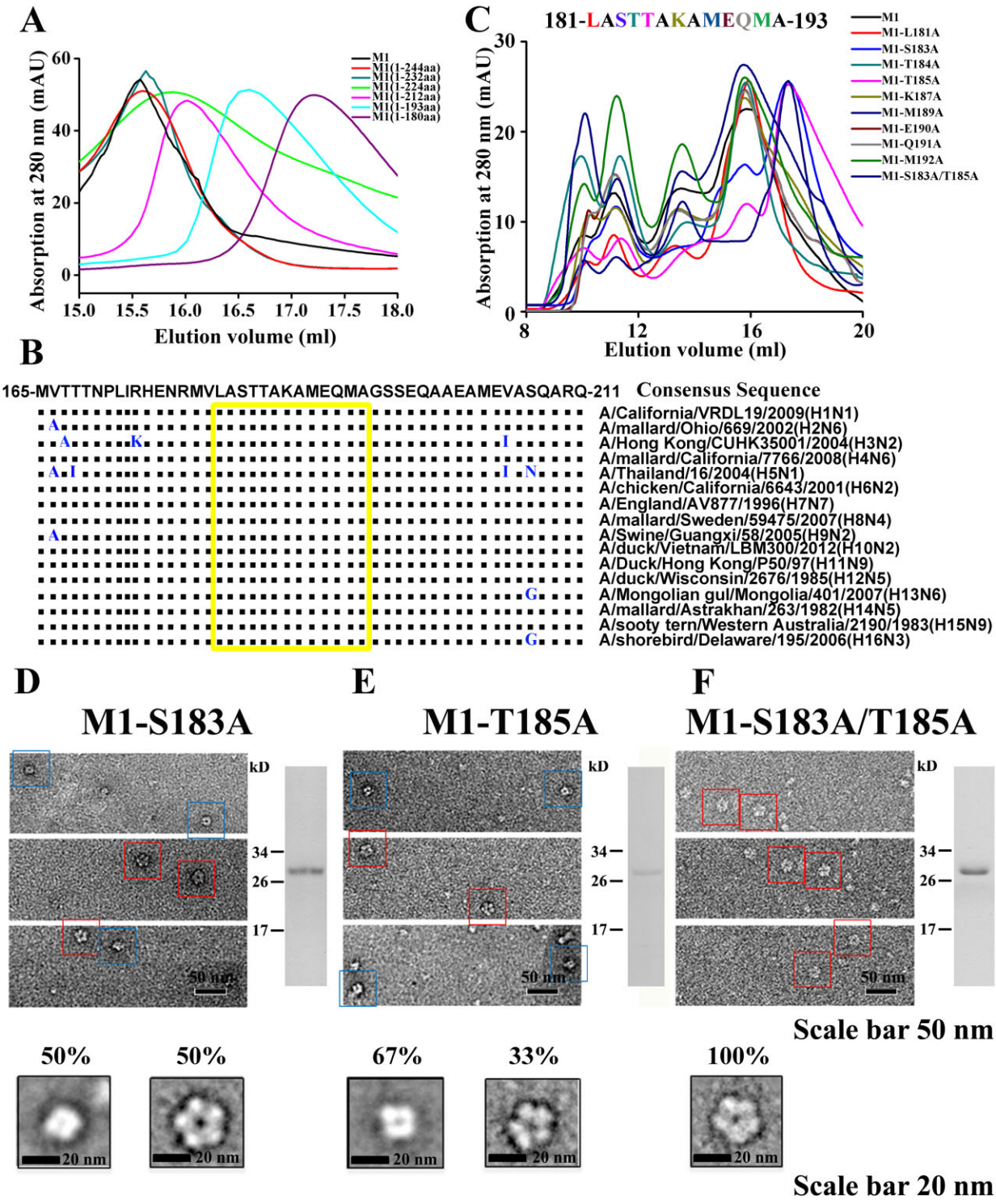

Fig. 2. S183 and T185 are key residues for the oligomerization pattern of M1.
A. Gel filtration analysis of the smallest oligomerization state of different C-terminal truncations of M1 at pH 7.4.
B. Conservation of the dimerization region. The conservation of 181–193 aa was solved by sequence alignment of the C-terminal domain of M1 in all subtypes of influenza A. The highlighted column indicates the high degree of conservation of this region.
C. Gel filtration analysis of M1 point mutants at the region of 181–193 aa at pH 7.4. The elution volumes of the smallest oligomerization states of each mutant are shown in different colours. Negative staining electron microscopy was used to examine the oligomerization pattern of M1-S183A (D), M1-T185A (E) and the M1-S183A/T185A double-point mutant (F). Each purified mutant protein was analysed by SDS-PAGE. Selected particles of each mutant oligomer were followed by initial processing with EMAN1.8 and a range of two-dimensional class averages (50 particles per class). Fourfold symmetrical particles are denoted by blue boxes, while fivefold symmetrical particles are in red boxes.

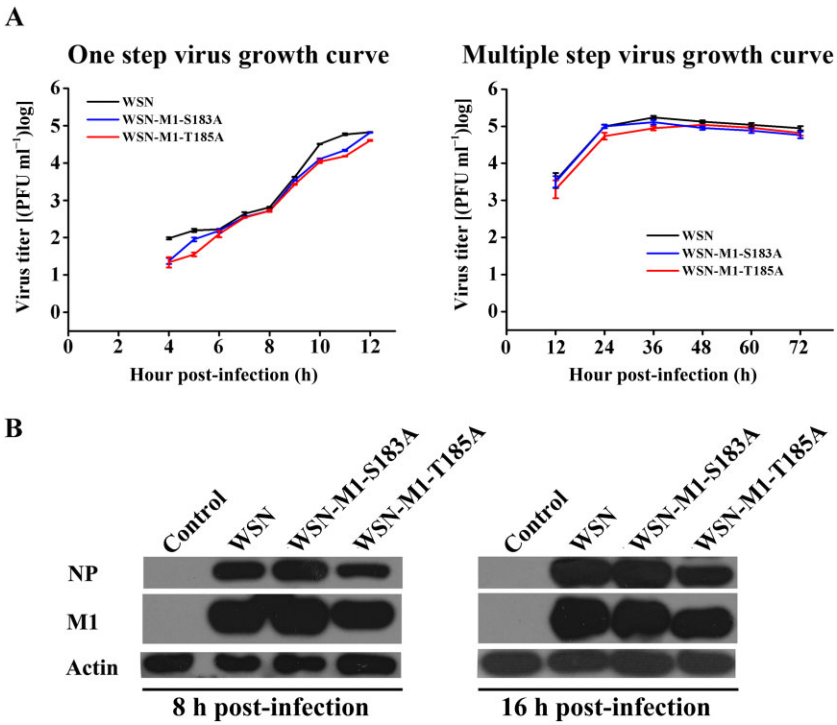

Fig. 3. Viral proteins in cells infected with M1 mutated virus.
A. The virus production rate was determined by one step growth curve (MOI = 0.1) and multistep growth curve (MOI = 0.001) of wild-type WSN and WSN containing M1 mutants infected MDCK cells. The culture supernatants collected at the indicated time points were subjected to plaque assays for virus titration. Error bars represent standard deviations of three independent experiments.
B. Detection the expression of viral proteins in virus-infected cells at 8 and 16 h post-infection by Western blotting with anti-NP polyclonal and anti-M1 monoclonal antibodies.

infected with the wild-type virus, most spherical shaped with few elongated virions were observed on the plasma membrane (Fig. 4B). In cells infected with either WSN-M1-S183A or WSN-M1-T185A, both spherical and filamentous particles were produced (Fig. 4C and D). But, unlike the filamentous viruses produced by wild-type (~ 100 nm wide), the width of the filamentous particles produced by M1 mutation was smaller (Fig. 4C and D). Then, the particles generated from repeated assay were collected from the cell supernatants, purified by ultracentrifugation and then analysed by negative staining electron microscopy. The results showed that wild-type virus particles were spherically shaped (Fig. 5A). However, elongated and filamentous particles were observed in the M1 mutant virus samples. One hundred viral particles of each virus from two independent experiments were used for statistical analysis. The result showed that the ratio of filamentous particles in WSN-M1-S183A was 19%. The average width of these filamentous particles was about 55 nm, nearly similar to the classical filamentous virus A/Udorn/72 (~ 60 nm wide) (Calder *et al.*, 2010; Fig. 5B). The filamentous virus particles produced by WSN-M1-T185A mutant virus only occupied 8% in the total amount of generated virus. The average width of M1-T185A mutant filamentous virus particles was about 80 nm (Fig. 5C). These results showed that single-point mutation at M1-S183 or M1-T185 could produce filamentous particles.

Because the mutation of S183 or T185 changes the oligomerization pattern of M1 (Fig. 3), the oligomerization pattern of M1, in turn, determined the organization of the matrix layer and the morphology of virions. These results showed that the oligomerization pattern of M1 determines the morphology of the matrix layer.

Discussion

Oligomerization of matrix proteins plays a critical role in many virus assembly and budding processes. Nipah virus M protein oligomerizes to form Virus-like particles (VLPs) (Ciancanelli and Basler, 2006; Walpita *et al.*, 2011). Oligomerization of measles virus M protein promotes the release of virus particles (Pohl *et al.*, 2007) and oligomerization of Ebola virus VP40 controls the morphology of virus particles (Hoenen *et al.*, 2010). Borna virus M protein oligomerizes to form two-dimensional lattices during virus assembly and budding (Kraus *et al.*, 2005). Furthermore, the M proteins of Sendai virus and NDV are both able to elicit efficient particle budding from transfected cells by oligomerization (Ali and Nayak, 2000; Battisti *et al.*, 2012).

For influenza A virus, oligomerization of M1 protein plays a central role in virus assembly and budding. Ruigrok *et al.* reported that M1 monomers are 6 nm long rods (Ruigrok *et al.*, 1989; 2000). M1 tends to oligomerize soon after synthesis and forms an ordered helical matrix layer adjacent to the envelope in the virus particles (Schulze, 1972; Wu *et al.*, 2011). Analysis of the crystal structure of the N-terminal domain, as well as functional studies, demonstrates that the N-terminal domain mediates the

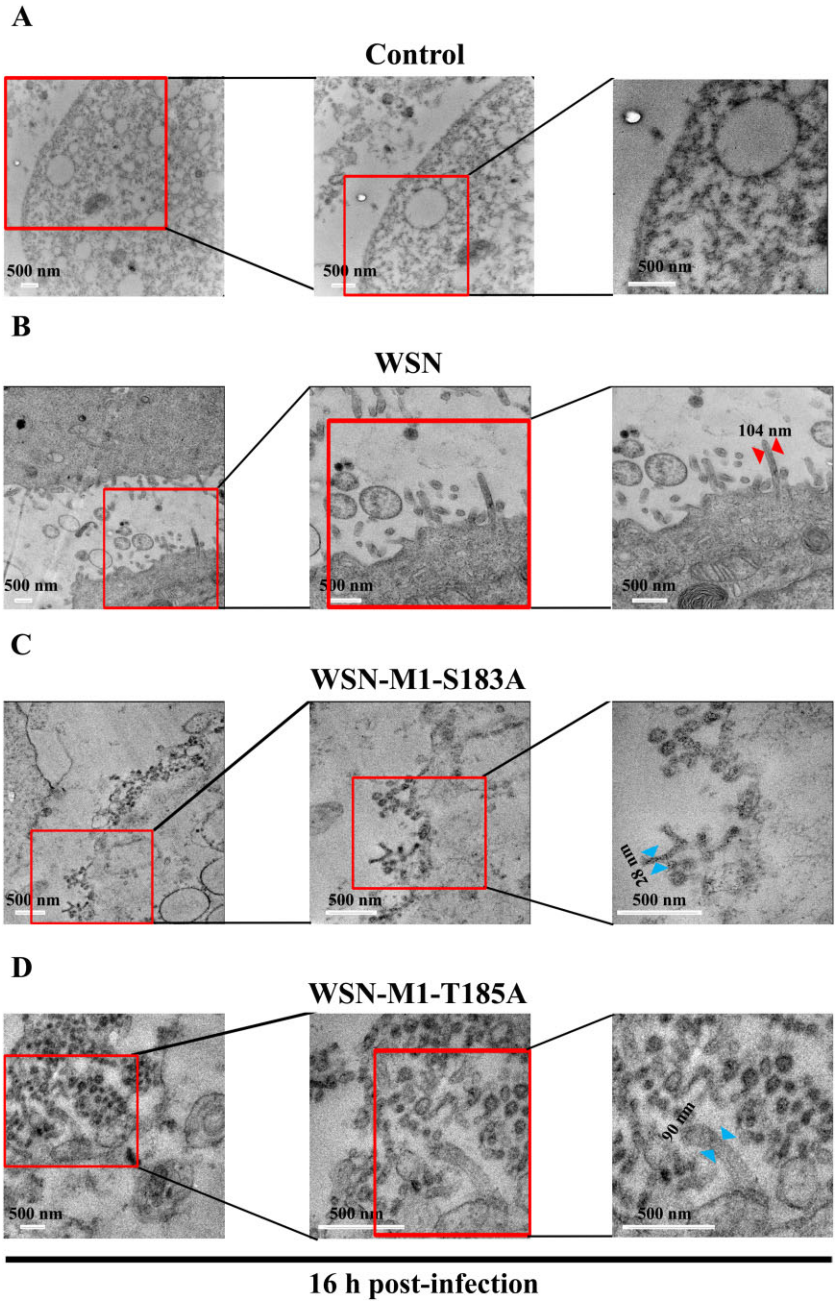

Fig. 4. M1-S183 and M1-T185 mutants affect virus morphology. Ultrastructural analysis of viruses was conducted by negative staining electron microscopy. MDCK cells uninfected (A) and infected with WSN viruses (B) or WSN-S183A virus (C) or WSN-T185A virus (D) at an MOI = 0.5 were examined by transmission electron microscopy at 16 h post-infection. The filamentous particles budding from surface of the cells are indicated by colourized arrows and their widths were calculated. Scale bars, 500 nm.

oligomerization of M1 (Harris *et al.*, 2001; Noton *et al.*, 2007).

In the present study, we investigated the oligomerization mechanism of M1 by detecting M1 oligomers from recombinant protein using negative staining microscopy. Particles from the 10.1 ml gel filtration fractions of M1 collected at neutral pH were identical, displaying fourfold symmetry. The molecular mass of the 10.1 ml fraction corresponds to 580 kDa. In contrast, particles from the 9.8 ml fraction of N-terminal domain, whose molecular mass was 650 kDa, displayed fivefold symmetry. It is necessary to clarify that the asymmetry units in two oligomers are not similar. 580-kDa ordered M1 oligomer (four-fold symmetry conformation) contains 20 copies of 29-kDa M1 monomers. There should be 5 copies of M1 monomer in each subdomain. 650 kDa ordered M1N oligomer (five-fold symmetry conformation) was approximately oligomerized by 30 copies of 20-kDa M1N monomer. Asymmetric subdomain in this oligomer conformation should have 6 copies of M1N monomer. Differentially organized oligomerization forms have also been observed for other virus matrix proteins. The Ebola virus matrix protein VP40, which also consists of N- and C-terminal domains connected by a flexible linker, can

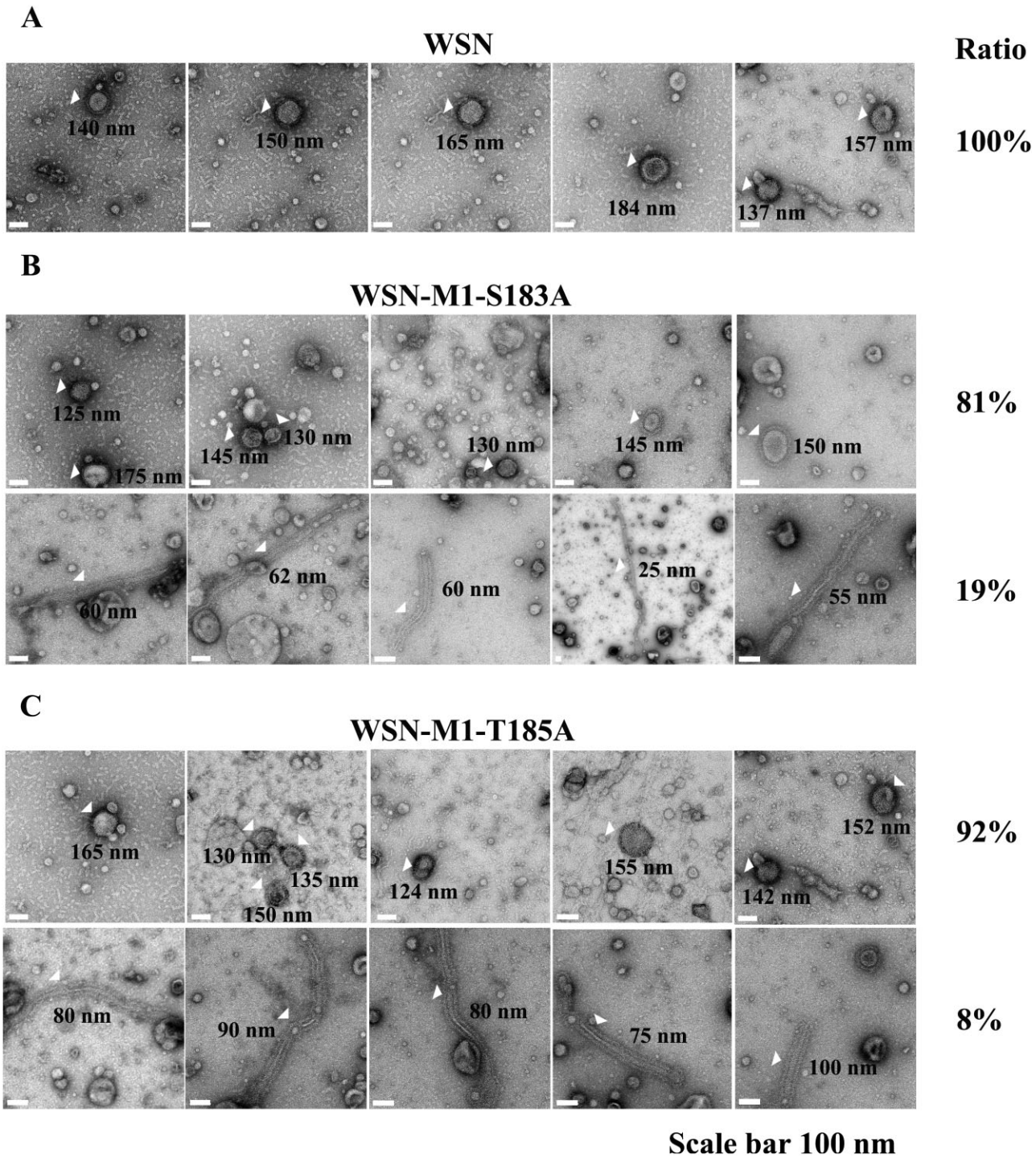

Fig. 5. The structures of purified virus particles. The viral particles generated by WSN (A) or WSN-S183A virus (B) or WSN-T185A virus (C) infecting MDCK cells were purified by ultracentrifugation and investigated by negative staining electron microscopy. The representative viral particles are shown by white arrows. The diameter of each representative particle is labelled. The ratio of spherical and filamentous after purified was calculated based on the statistics of 100 particles from two independent experiments. Scale bars, 100 nm.

oligomerize into hexamers and octamers (Hoenen *et al.*, 2010). Similar to M1, the N-terminus of VP40 is also the oligomerization domain of the intact protein (Nguyen *et al.*, 2005).

The N-terminal domain is the oligomerization domain of M1. Oligomers of the N-terminal domain display fivefold symmetry, so establishment of fourfold symmetry requires the participation of the C-terminal domain. The C-terminal

domain, for which three-dimensional structure has not been solved, contains a considerably flexible region that provides many possible protein-protein interaction sites. However, little about the function of the C-terminal domain has been reported. Recently, it was reported that K242 is a SUMOylation site that is responsible for the morphology of the virus particles (Wu *et al*., 2011). Previously, we reported that the C-terminal domain forms a stable dimer contributing to the oligomerization of M1 (Zhang *et al*., 2012). Recently, Shtykova *et al*. found that full-length M1 could not form supramolecular structure in the absence of C-terminal domain (Shtykova *et al*., 2013). Elton *et al*. found that one C-terminal domain mutation, N231D, could affect the morphology of equine influenza viruses by producing small filamentous structures (Elton *et al*., 2013). Therefore, C-terminal domain should play an important role in M1 self-oligomerization. By analysis of the oligomerization state and oligomerization pattern of several C-terminally truncated M1 proteins, we determined that the oligomerization pattern of intact M1 is controlled by residues 181–193, a highly conserved region in all subtypes of influenza A virus M1 protein.

Additional studies revealed that a polar-containing motif, 183-STT-185, which is in putative helix 11 of full-length protein (Shishkov *et al*., 1999; 2009; 2011; Shtykova *et al*., 2013), is essential for oligomerization pattern of M1. To date, no function for such polar residues has been reported in other viral matrix proteins. Here, we found that S183 and T185 are key residues for the oligomerization of M1. Single alanine point mutation in either of the two residues partially inhibited the dimerization of M1, causing both fourfold and fivefold symmetrical particles to appear in the M1 oligomers. As a result, both spherical and filamentous morphological viral particles could be produced in WSN-M1-S183A and WSN-M1-T185A mutant virus. The double alanine mutant completely destroyed the dimerization of M1, causing the formation of M1 oligomers with only fivefold symmetry. But M1-S183A/T185A did not support virus production, maybe due to other functional role of this motif. It has been reported that the 183-STT-185 motif is a target of phosphokinase C (Reinhardt and Wolff, 2000). Therefore, the other functional roles of this hydroxyl groups should be further studied. The multifunctional roles of 183-STT-185 motif may give us new concept on the novel antiviral drug design targeting the M1 protein.

In summary, we studied the molecular mechanism of the oligomerization of the influenza A virus M1 protein and found key C-terminal region that controls the oligomerization pattern of M1. Two polar residues in this highly conserved region, S183 and T183, play key roles in the M1 oligomerization pattern and virus budding. The present data provide new insights into the mechanism of the formation of the matrix layer and help us to better understand the budding process of influenza A virus.

Experimental procedures

Reagents, plasmids, antibodies, bacterial strains and cells lines

A QuikChange II Site-Directed Mutagenesis Kit, Lipofectamine 2000, Dulbecco's modified Eagle medium (DMEM) and GIBCO fetal bovine serum were obtained from Invitrogen. Carbon-coated grids were obtained from Quantifoil. Mouse anti-M1 monoclonal antibody and rabbit anti-NP or anti-HA polyclonal antibody were prepared by standard procedures. The origin of other materials was described in the previous study (Zhang *et al*., 2012).

Recombinant plasmid construction

All proteins used in this study were expressed from recombinant plasmids in *E. coli*. The construction of recombinant plasmids pET30a-M1 and pET30a-M1N is described in a previous study (Zhang *et al*., 2012). The plasmid fragments encoding M1 amino acids 1–180, 1–193, 1–212, 1–224, 1–232 and 1–244 were subcloned into the *Nde*I and *Xho*I sites of pET30a, generating plasmids pET30a-M1-180, pET30a-M1-193, pET30a-M1-212, pET30a-M1-224, pET30a-M1-232 and pET30a-M1-224, containing a His_6 tag coding sequence fused at the C-terminus. All of the abovementioned constructs were transformed into *E. coli* strain DH5α and the inserted genes were confirmed by DNA sequencing.

The amino acid substitutions were introduced to the aforementioned constructed plasmids using a QuikChange II site-directed mutagenesis kit. The positions of the mutations included L181, S183, T184, T185, K187, M189, E190, Q191 and M192. The generation of the S183/T185 double mutant occurred by introducing the T185 mutation into the S183-mutated cDNA. Amplification was performed by polymerase chain reaction (PCR) with *Pfu* polymerase and primers containing the appropriate base changes generating plasmids pET-30a-M1-L181A, pET-30a-M1-S183A, pET-30a-M1-T184A, pET-30a-M1-T185A, pET-30a-M1-K187A, pET-30a-M1-M189A, pET-30a-M1-E190A, pET-30a-M1-Q191A, pET-30a-M1-M192A, pET-30a-M1-S183A/T185A. pHH21-M1-S183A, pHH21-M1-T185A and pHH21-M1-S183A/T185A derived from pHH21-M1 in the 12 plasmid system of A/WSN/1933 virus. The resulting plasmids with the desired mutations were confirmed by sequence analysis.

Protein expression and purification

The recombinant pET30a-M1 along with its relevant mutant and truncation versions were separately expressed in *E. coli* strain BL21 (DE3) in the presence of 0.5 mM isopropyl-1-thio-β-D-galactopyranoside for 11 h at 16°C. The two steps purification of each protein followed the same procedure as described previously (Zhang *et al*., 2012). The apparent molecular masses of the fractions on gel filtration column were estimated based on the acquired standard curve. Protein samples from affinity chromatography and peak fractions from gel filtration were examined by 12% Sodium dodecyl sulfate Polyacrylamide gel electrophoresis (SDS-PAGE) and visualized by staining with Coomassie blue. The determination of the smallest oligomerization state of the recombinant proteins was performed on the Superdex™ 200 column in 20 mM Tris (pH 7.4) and 150 mM NaCl, controlled by

an AKTA Fast protein liquid chromatography (FPLC) system. The processes were the same as described previously (Zhang *et al.*, 2012).

Cell culture

The 293T cells and MDCK cells were maintained in DMEM supplemented with 10% fetal bovine serum at 37°C in a 10% CO_2 atmosphere.

Reverse genetics

The wild-type WSN virus and M1 mutant viruses were generated using the 12 plasmid reverse genetics system (Neumann *et al.*, 1999). Briefly, 293T cells grown in 60 mm dishes to 90% confluence were transfected with 0.5 μg of plasmids each. A total of 6 μg DNA was transfected using 15 μl Lipofectamine 2000. At 16 h post-transfection, 0.5 μg ml^{-1} of tosyl-phenylalanine chloromethyl-ketone (TPCK)-trypsin was added to the cells. The culture supernatant was then harvested 60 h post-transfection. Next, the supernatant was clarified and added to fresh MDCK cells to amplify the virus. To identify the M1 mutations, the vRNA extracted from the recovered virus in culture supernatant was sequenced. The recovered viruses were named based on their mutated M1 as follows: WSN-M1-S183A and WSN-M1-T185A.

Plaque assay

Virus titers were determined by plaque assays. MDCK cells cultured in 12-well tissue culture dishes were washed with Phosphate-buffered saline (PBS) and infected with virus for 1 h at 37°C. The virus inoculum was then removed by washing with PBS. Next, cell monolayers were overlaid with agar overlay medium (DMEM supplemented with 3% low melting point agarose and 2 μg of TPCK-treated trypsin ml^{-1}) and incubated at 4°C for 20 min until the medium was solidified. Then, the dishes were incubated at 37°C. Visible plaques were counted at 3 days post-infection. All data are expressed as the means of three independent experiments. Then, the plaque assays were performed to determine virus growth kinetics at a multiplicity of infection (MOI) of 0.1 or 0.001.

Western blotting

Transfected cells or infected cells were lysed with lysis buffer [0.5% NP-40, 150 mM NaCl, 20 mM 4-(2-hydroxyethyl)-1-piperazineethanesulfonic acid (HEPES) (pH 7.4), 10% glycerol and 1 mM Ethylenediaminetetraacetic acid (EDTA) with complete protease inhibitor cocktail] and subjected to Western blotting. Protein samples were separated by 12% SDS-PAGE and transferred to Polyvinylidene fluoride (PVDF) membranes. The membranes were blocked overnight at 4°C in blocking solution (Tris-Buffered Saline and Tween 20 (TBST) supplemented with 5% skim milk powder and Bovine serum albumin (BSA)) and proteins were detected using appropriate primary antibodies: anti-M1 mouse monoclonal (1:1000), anti-NP rabbit polyclonal (1:2000) and anti-β-actin mouse monoclonal (1:2500) antibodies. After several washing steps (TBST), the membranes were incubated with anti-rabbit or anti-mouse secondary antibody (1:5000) coupled to horseradish peroxidase (HRP). The HRP-linked antibodies were visualized by enhanced chemiluminescence detection as described by the manufacturer.

Transmission electron microscopy, image processing and analysis

The 10.1 ml (580 kDa) fraction of M1 and the 9.8 ml (654 kDa) fraction of M1N were collected from the gel filtration column in 20 mM Tris (pH 7.4) and 150 mM NaCl and applied to carbon-coated copper grids. The samples were negatively stained with 2% uranyl acetate for 1 min and the excess liquid was wicked off. The grids were dried at room temperature overnight and observed in a JEOL1400 transmission electron microscope operating at 80 kV. Images were taken at a nominal magnification of 60 000 × over a range of nominal defocus (1.5–2.5 μm) on a 1 k × 1 k Charge Coupled Device (CCD) camera with a pistol size value of 4 Å. Representative images of protein particles were selected using the 'boxer' program of the image processing software EMAN (Goddard *et al.*, 2007).

Ultra-thin section electron microscopy was performed as described previously. Briefly, uninfected MDCK cells and MDCK cells infected with WSN or WSN-M1-S183A or WSN-M1-T185A viruses at MOI 0.5 were fixed with 3% glutaraldehyde in 0.1 M cacodylate buffer at 16 h post-infection and post-fixed with 2% osmium tetroxide in the same buffer. Cells were then dehydrated with a series of ethanol gradients followed by propylene oxide. Each assay was repeated twice. Thin sections were stained with 2% uranyl acetate and Raynold's lead and examined under a JEOL1400 electron microscope at 80 kV.

The supernatant from the assay mentioned previously was collected, purified by ultracentrifugation and resuspended in PBS. Then, each sample containing two repeats was negatively stained with 2% uranyl acetate for 1 min and observed in a JEOL1400 transmission electron microscope operating at 80 kV.

Acknowledgements

This work was supported by the National Key Technologies Research and Development Program of China (2013ZX10004-610), Chinese National 973 Program (2012CB518903, 2012CB955501 and 2011CB504705 to W.-J.L. and 2010CB912400 and 2012CB917200 to C.-C.Y.), the National Natural Science Foundation of China (31101830, 81101253 and 81101254), Intramural special grant for influenza virus research from the Chinese Academy of Sciences (KJZD-EW-L09-2), the Key Research Program of the Chinese Academy of Sciences (KSZD-EW-Z-005-001 and KSCX2-EW-Q-14) and International development research center (IDRC) Project Funding. Dr. W.-J.L. is the principal investigators of the Innovative Research Group of the National Natural Science Foundation of China (grant number 81321063).

References

Ali, A., and Nayak, D.P. (2000) Assembly of Sendai virus: M protein interacts with F and HN proteins and with the cytoplasmic tail and transmembrane domain of F protein. *Virology* **276:** 289–303.

Ali, A., Avalos, R.T., Ponimaskin, E., and Nayak, D.P. (2000) Influenza virus assembly: effect of influenza virus glycoproteins on the membrane association of M1 protein. *J Virol* **74:** 8709–8719.

Arzt, S., Baudin, F., Barge, A., Timmins, P., Burmeister, W.P., and Ruigrok, R.W. (2001) Combined results from solution studies on intact influenza virus M1 protein and from a new crystal form of its N-terminal domain show that M1 is an elongated monomer. *Virology* **279:** 439–446.

Avalos, R.T., Yu, Z., and Nayak, D.P. (1997) Association of influenza virus NP and M1 proteins with cellular cytoskeletal elements in influenza virus-infected cells. *J Virol* **71:** 2947–2958.

Barman, S., Ali, A., Hui, E.K., Adhikary, L., and Nayak, D.P. (2001) Transport of viral proteins to the apical membranes and interaction of matrix protein with glycoproteins in the assembly of influenza viruses. *Virus Res* **77:** 61–69.

Battisti, A.J., Meng, G., Winkler, D.C., McGinnes, L.W., Plevka, P., Steven, A.C., *et al*. (2012) Structure and assembly of a paramyxovirus matrix protein. *Proc Natl Acad Sci USA* **109:** 13996–14000.

Bialas, K.M., Desmet, E.A., and Takimoto, T. (2012) Specific residues in the 2009 H1N1 swine-origin influenza matrix protein influence virion morphology and efficiency of viral spread in vitro. *PloS one* **7:** e50595.

Bui, M., Wills, E.G., Helenius, A., and Whittaker, G.R. (2000) Role of the influenza virus M1 protein in nuclear export of viral ribonucleoproteins. *Journal of virology* **74:** 1781–1786.

Burleigh, L.M., Calder, L.J., Skehel, J.J., and Steinhauer, D.A. (2005) Influenza a viruses with mutations in the m1 helix six domain display a wide variety of morphological phenotypes. *Journal of virology* **79:** 1262–1270.

Calder, L.J., Wasilewski, S., Berriman, J.A., and Rosenthal, P.B. (2010) Structural organization of a filamentous influenza A virus. *Proceedings of the National Academy of Sciences of the United States of America* **107:** 10685–10690.

Ciancanelli, M.J., and Basler, C.F. (2006) Mutation of YMYL in the Nipah virus matrix protein abrogates budding and alters subcellular localization. *Journal of virology* **80:** 12070–12078.

Elleman, C.J., and Barclay, W.S. (2004) The M1 matrix protein controls the filamentous phenotype of influenza A virus. *Virology* **321:** 144–153.

Elton, D., Bruce, E.A., Bryant, N., Wise, H.M., MacRae, S., Rash, A., *et al*. (2013) The genetics of virus particle shape in equine influenza A virus. *Influenza and other respiratory viruses* **7** (Suppl. 4)**:** 81–89.

Enami, M., Fukuda, R., and Ishihama, A. (1985) Transcription and replication of eight RNA segments of influenza virus. *Virology* **142:** 68–77.

Ge, P., Tsao, J., Schein, S., Green, T.J., Luo, M., and Zhou, Z.H. (2010) Cryo-EM model of the bullet-shaped vesicular stomatitis virus. *Science* **327:** 689–693.

Goddard, T.D., Huang, C.C., and Ferrin, T.E. (2007) Visualizing density maps with UCSF Chimera. *J Struct Biol* **157:** 281–287.

Gomez-Puertas, P., Albo, C., Perez-Pastrana, E., Vivo, A., and Portela, A. (2000) Influenza virus matrix protein is the major driving force in virus budding. *J Virol* **74:** 11538–11547.

Harris, A., Forouhar, F., Qiu, S., Sha, B., and Luo, M. (2001) The crystal structure of the influenza matrix protein M1 at neutral pH: M1-M1 protein interfaces can rotate in the oligomeric structures of M1. *Virology* **289:** 34–44.

Heggeness, M.H., Smith, P.R., Ulmanen, I., Krug, R.M., and Choppin, P.W. (1982) Studies on the helical nucleocapsid of influenza virus. *Virology* **118:** 466–470.

Hoenen, T., Biedenkopf, N., Zielecki, F., Jung, S., Groseth, A., Feldmann, H., and Becker, S. (2010) Oligomerization of Ebola virus VP40 is essential for particle morphogenesis and regulation of viral transcription. *J Virol* **84:** 7053–7063.

Kraus, I., Bogner, E., Lilie, H., Eickmann, M., and Garten, W. (2005) Oligomerization and assembly of the matrix protein of Borna disease virus. *FEBS Lett* **579:** 2686–2692.

Ksenofontov, A.L., Dobrov, E.N., Fedorova, N.V., Radiukhin, V.A., Badun, G.A., Arutiunian, A.M., *et al*. (2011) [Disordered regions in C-domain structure of influenza virus M1 protein]. *Mol Biol (Mosk)* **45:** 689–696.

Lamb, R.A., and Choppin, P.W. (1983) The gene structure and replication of influenza virus. *Annu Rev Biochem* **52:** 467–506.

Latham, T., and Galarza, J.M. (2001) Formation of wild-type and chimeric influenza virus-like particles following simultaneous expression of only four structural proteins. *J Virol* **75:** 6154–6165.

Liljeroos, L., Huiskonen, J.T., Ora, A., Susi, P., and Butcher, S.J. (2011) Electron cryotomography of measles virus reveals how matrix protein coats the ribonucleocapsid within intact virions. *Proc Natl Acad Sci USA* **108:** 18085–18090.

Nayak, D.P., Hui, E.K., and Barman, S. (2004) Assembly and budding of influenza virus. *Virus Res* **106:** 147–165.

Nayak, D.P., Balogun, R.A., Yamada, H., Zhou, Z.H., and Barman, S. (2009) Influenza virus morphogenesis and budding. *Virus Res* **143:** 147–161.

Neumann, G., Watanabe, T., Ito, H., Watanabe, S., Goto, H., Gao, P., *et al*. (1999) Generation of influenza A viruses entirely from cloned cDNAs. *Proc Natl Acad Sci USA* **96:** 9345–9350.

Nguyen, T.L., Schoehn, G., Weissenhorn, W., Hermone, A.R., Burnett, J.C., Panchal, R.G., *et al*. (2005) An all-atom model of the pore-like structure of hexameric VP40 from Ebola: structural insights into the monomer-hexamer transition. *J Struct Biol* **151:** 30–40.

Noton, S.L., Medcalf, E., Fisher, D., Mullin, A.E., Elton, D., and Digard, P. (2007) Identification of the domains of the influenza A virus M1 matrix protein required for NP binding, oligomerization and incorporation into virions. *J Gen Virol* **88:** 2280–2290.

Pohl, C., Duprex, W.P., Krohne, G., Rima, B.K., and Schneider-Schaulies, S. (2007) Measles virus M and F proteins associate with detergent-resistant membrane fractions and promote formation of virus-like particles. *J Gen Virol* **88:** 1243–1250.

Reinhardt, J., and Wolff, T. (2000) The influenza A virus M1 protein interacts with the cellular receptor of activated C kinase (RACK) 1 and can be phosphorylated by protein kinase C. *Vet Microbiol* **74:** 87–100.

Rossman, J.S., Jing, X., Leser, G.P., Balannik, V., Pinto, L.H., and Lamb, R.A. (2010) Influenza virus m2 ion channel protein is necessary for filamentous virion formation. *J Virol* **84:** 5078–5088.

Ruigrok, R.W., Calder, L.J., and Wharton, S.A. (1989) Electron microscopy of the influenza virus submembranal structure. *Virology* **173:** 311–316.

Ruigrok, R.W., Barge, A., Durrer, P., Brunner, J., Ma, K., and Whittaker, G.R. (2000) Membrane interaction of influenza virus M1 protein. *Virology* **267:** 289–298.

Schulze, I.T. (1972) The structure of influenza virus. II. A model based on the morphology and composition of subviral particles. *Virology* **47:** 181–196.

Sha, B., and Luo, M. (1997a) Crystallization and preliminary X-ray crystallographic studies of type A influenza virus matrix protein M1. *Acta Crystallogr D Biol Crystallogr* **53:** 458–460.

Sha, B., and Luo, M. (1997b) Structure of a bifunctional membrane-RNA binding protein, influenza virus matrix protein M1. *Nat Struct Biol* **4:** 239–244.

Shaw, M.L., Stone, K.L., Colangelo, C.M., Gulcicek, E.E., and Palese, P. (2008) Cellular proteins in influenza virus particles. *PLoS Pathog* **4:** e1000085.

Shishkov, A., Bogacheva, E., Fedorova, N., Ksenofontov, A., Badun, G., Radyukhin, V., *et al*. (2011) Spatial structure peculiarities of influenza A virus matrix M1 protein in an acidic solution that simulates the internal lysosomal medium. *FEBS J* **278:** 4905–4916.

Shishkov, A.V., Goldanskii, V.I., Baratova, L.A., Fedorova, N.V., Ksenofontov, A.L., Zhirnov, O.P., and Galkin, A.V. (1999) The in situ spatial arrangement of the influenza A virus matrix protein M1 assessed by tritium bombardment. *Proc Natl Acad Sci USA* **96:** 7827–7830.

Shishkov, A.V., Bogacheva, E.N., Dolgov, A.A., Chulichkov, A.L., Knyazev, D.G., Fedorova, N.V., *et al*. (2009) The in situ structural characterization of the influenza A virus matrix M1 protein within a virion. *Protein Pept Lett* **16:** 1407–1413.

Shtykova, E.V., Baratova, L.A., Fedorova, N.V., Radyukhin, V.A., Ksenofontov, A.L., Volkov, V.V., *et al*. (2013) Structural analysis of influenza A virus matrix protein m1 and its self-assemblies at low pH. *PLoS ONE* **8:** e82431.

Walpita, P., Barr, J., Sherman, M., Basler, C.F., and Wang, L. (2011) Vaccine potential of Nipah virus-like particles. *PLoS ONE* **6:** e18437.

Wang, D., Harmon, A., Jin, J., Francis, D.H., Christopher-Hennings, J., Nelson, E., *et al*. (2010) The lack of an inherent membrane targeting signal is responsible for the failure of the matrix (M1) protein of influenza A virus to bud into virus-like particles. *J Virol* **84:** 4673–4681.

Wu, C.Y., Jeng, K.S., and Lai, M.M. (2011) The SUMOylation of matrix protein M1 modulates the assembly and morphogenesis of influenza A virus. *J Virol* **85:** 6618–6628.

Zhang, K., Wang, Z., Liu, X., Yin, C., Basit, Z., Xia, B., and Liu, W. (2012) Dissection of influenza A virus M1 protein: pH-dependent oligomerization of N-terminal domain and dimerization of C-terminal domain. *PLoS ONE* **7:** e37786.

